

Order-by-disorder charge density wave condensation at $q = (\frac{1}{3}, \frac{1}{3}, \frac{1}{3})$ in kagome metal ScV_6Sn_6

Alaska Subedi

CPHT, CNRS, École polytechnique, Institut Polytechnique de Paris, 91120 Palaiseau, France

(Dated: August 24, 2023)

The recent discovery of a charge density wave order at the wave vector $P (\frac{1}{3}, \frac{1}{3}, \frac{1}{3})$ in the kagome metal ScV_6Sn_6 has created a mystery because subsequent theoretical and experimental studies show a dominant phonon instability instead at another wave vector $H (\frac{1}{3}, \frac{1}{3}, \frac{1}{2})$. In this paper, I use first principles total energy calculations to map out the landscape of the structural distortions due to the unstable phonon modes at H , $L (\frac{1}{2}, 0, \frac{1}{2})$, and P present in this material. In agreement with previous results, I find that the distortions due to the H instability cause the largest gain in energy relative to the parent structure, followed in order by the L and P instabilities. However, only two distinct structure occur due to this instability, which are separated by 6 meV/f.u. The instability at L results in three distinct structures separated in energy by 5 meV/f.u. In contrast, six different distorted structures are stabilized due to the instability at P , and they all lie within 2 meV/f.u. of each other. Hence, despite a lower energy gain, the condensation at P could be favorable due to a larger entropy gain associated with the fluctuations within a manifold with larger multiplicity via the order-by-disorder mechanism.

I. INTRODUCTION

Materials that have the kagome lattice as their structural motif have been well studied in the context of frustrated magnetism [1]. The frustrated lattice also gives rise to remarkable electronic structure with Dirac cones and flat bands [2–5]. Various emergent phases due to electronic instabilities in these materials have been anticipated [6–11], and the discovery of charge density wave (CDW) order in kagome metals AV_3Sb_5 ($A = \text{K}, \text{Rb}, \text{Cs}$) and FeGe has motivated further exploration of this class of materials for uncommon ground states and excitations [12, 13].

A notable result of this activity is Suriya Arachchige *et al.*'s discovery of first-order CDW transition in the bilayer kagome metal ScV_6Sn_6 at the wave vector $P (\frac{1}{3}, \frac{1}{3}, \frac{1}{3})$ [14], which is highly unusual because P is not a high-symmetry point in the Brillouin zone where dense scattering phase space is usually expected. Angle resolved photoemission and optical spectroscopy experiments across the transition show relatively modest electronic structure changes at the Fermi level with no gap opening [15–22], which indicates that an electronic instability does not cause the CDW transition. Intriguingly, inelastic x-ray scattering (IXS) experiments find that the lowest-frequency phonon mode at P softens only modestly as the transition temperature $T_c = 92$ K is approached from above [20, 23], while a phonon mode at another wave vector $H (\frac{1}{3}, \frac{1}{3}, \frac{1}{2})$ softens completely to zero [20]. Diffuse scattering signals that grow in intensity from room temperature to 100 K is observed around H , whereas no such signals are seen around the ordering wave vector P [20, 23, 24]. Calculated phonon dispersion find an unstable branch that has the largest imaginary frequency at H [25], seemingly in agreement with the IXS experiments. However, the calculated energy gain due to the instability at H is also larger than that due to the one at P . This suggests that a mechanism beyond

the harmonic level in atomic displacements may be necessary to describe the CDW transition observed in this material, although the energetics of all possible distorted structures due to these phonon instabilities has not been thoroughly investigated.

In this paper, I study the energetics of structural distortions in ScV_6Sn_6 using group theory and density functional theory (DFT) calculations. Group-theoretical analysis was utilized to enumerate the possible symmetrically-distinct distortions in the order parameter subspaces described by the phonon instabilities at H , $L (\frac{1}{2}, 0, \frac{1}{2})$, and P . Calculated eigenvectors of these phonon instabilities were then used to generate the distorted structures, and their total energies were obtained from DFT after full relaxations that minimized both the lattice stresses and atomic forces. Consistent with previous results, I find that a distorted structure due to the instability at H has the lowest energy. I was also able to stabilize six symmetrically-distinct structures due to the instability at P whose calculated total energies lie within 2 meV/f.u. of each other. Fluctuations among these nearly-degenerate states likely stabilize the CDW order at P via the order-by-disorder mechanism. Experimental confirmation of the presence of these nearly-degenerate states by, for example, counting the number of domains in the low-temperature phase would strengthen the case that entropic force is responsible for the structural transition observed in this material.

II. COMPUTATIONAL APPROACH

The phonon dispersions and structural relaxation calculations presented here were performed using the pseudopotential-based QUANTUM ESPRESSO package [26] within the optB88-vdW approximation for the exchange-correlation functional [27]. I used the pseudopotentials generated by Dal Corso [28] and plane-wave

cutoffs of 60 and 600 Ry for the basis-set and charge density expansions, respectively. The Brillouin zone integration was performed using a $12 \times 12 \times 6$ k -point grid for the parent 13-atom structure. Equivalent or denser grids were used for the calculations on supercells. A 0.01 Ry Marzari-Vanderbilt smearing was used to determine the partial occupancies. The dynamical matrices of the parent structure were calculated on a $6 \times 6 \times 6$ q -point grid using density functional perturbation theory [29].

I used the ISOTROPY code [30] to determine the order parameter directions of all possible distortions due to the unstable phonon modes at H , L and P , as well as the number of domains exhibited by the distorted structures. The calculated phonon eigenvectors of the unstable modes were used to generate the distorted structures corresponding to the isotropy subgroups on the supercells commensurate with the phonon wave vectors, which were then fully relaxed by minimizing both the lattice stresses and atomic forces. I made extensive use of the FINDSYM [31] and SPGLIB [32] codes in the symmetry analysis of the calculated structures. The AMPLIMODES code [33] was used to determine the order parameter amplitudes of the relaxed structure. The polynomial expansion of the free energy as a function of the order parameters were performed using the INVARIANTS code [34].

III. RESULTS AND DISCUSSION

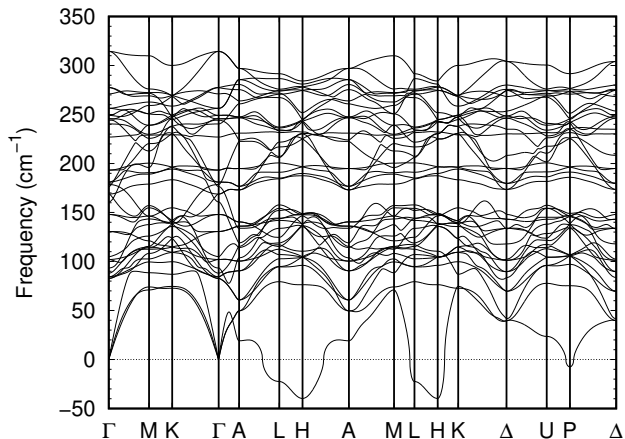


FIG. 1. Calculated phonon dispersions of fully-relaxed ScV_6Sn_6 in the parent $P6/mmm$ phase obtained using the optB88-vdW functional. The high-symmetry points are Γ (0, 0, 0), M ($\frac{1}{2}$, 0, 0), K ($\frac{1}{3}$, $\frac{1}{3}$, 0), A (0, 0, $\frac{1}{2}$), L ($\frac{1}{2}$, 0, $\frac{1}{2}$), H ($\frac{1}{3}$, $\frac{1}{3}$, $\frac{1}{2}$), Δ (0, 0, $\frac{1}{3}$), U ($\frac{1}{2}$, 0, $\frac{1}{3}$), P ($\frac{1}{3}$, $\frac{1}{3}$, $\frac{1}{3}$). Imaginary frequencies are denoted by negative values.

The calculated phonon dispersions of ScV_6Sn_6 in the high-temperature $P6/mmm$ structure obtained using the optB88-vdW functional is shown in Fig. 1. As in previously published results [19–21, 23, 25], there is a non-degenerate branch that is unstable along the path L - H

and at P . The largest instability occurs at H with a calculated imaginary frequency of $40i \text{ cm}^{-1}$. For comparison, the calculated values at L and P are $22i$ and $7i \text{ cm}^{-1}$, respectively. These results are somewhat in agreement with the inelastic x-ray scattering experiment of Korshunov *et al.* in that they observe a complete softening of the phonon mode at H as T_c is approached from above, whereas the phonons at L and P exhibit only a weak softening [20]. However, these are incongruent with the fact that the CDW order stabilizes at P , where the calculated instability is the weakest. The gain in energy due to the structural distortion at P could in principle be larger than the one at H as a result of additional freezing of secondary order parameters. But full structural relaxations by Tan and Yan show that the distorted structure due to the instability at H is lower in energy than the one due to the instability at P [25].

TABLE I. Isotropy subgroups and order parameter directions (OPD) of $P6/mmm$ for the irreps H_3 , L_2^- , and P_1 . Total energies of the fully-relaxed structures corresponding to these order parameters are given in the units of meV per formula unit relative to the parent $P6/mmm$ phase. Note that the order parameters refer to that of the initial structure before the minimization of stresses and forces. Symmetry-allowed secondary order parameters appear for the final relaxed structures. Not all distortions could be stabilized. Full structural information of all the phases that could be stabilized is given in Supplemental Material [35].

Space group (No.)	OPD	Energy (meV/f.u.)
$P6/mmm$ (191)	$H_3(a, 0)$	-16.68
$P6_3/mmc$ (194)	$H_3(0, a)$	-10.64
$P\bar{6}m2$ (187)	$H_3(a, b)$	—
$Immm$ (71)	$L_2^-(a, 0, 0)$	-12.10
$Fmmm$ (69)	$L_2^-(a, -a, 0)$	-4.01
$P6/mmm$ (191)	$L_2^-(a, a, a)$	-7.50
$C2/m$ (12)	$L_2^-(a, b, 0)$	—
$Cmmm$ (65)	$L_2^-(a, b, a)$	—
$P2/m$ (10)	$L_2^-(a, b, c)$	—
$R\bar{3}m$ (166)	$P_1(a, 0, 0, 0)$	-3.07
$R\bar{3}m$ (166)	$P_1(-a, 0, 0, 0)$	-1.17
$P6/mmm$ (191)	$P_1(a, 0, a, 0)$	-2.18
$P6/mmm$ (191)	$P_1(-a, 0, -a, 0)$	-1.76
$P6mm$ (183)	$P_1(a, b, a, b)$	-2.20
$P6mm$ (183)	$P_1(-a, -b, -a, -b)$	-1.92
$R\bar{3}m$ (160)	$P_1(a, b, 0, 0)$	—
$P\bar{6}m2$ (187)	$P_1(a, b, a, -b)$	—
$P\bar{3}m1$ (164)	$P_1(a, 0, b, 0)$	—
$P\bar{3}m1$ (156)	$P_1(a, b, c, d)$	—

Previous structural relaxation studies report only one distorted structure due to the instability at P [23, 25, 36], and it is possible that another distorted structure at P lies at the global minimum in the energy landscape. In fact, even though the unstable phonon branch is non-degenerate, the order parameter subspaces due to the instabilities at H , L , and P are multidimensional because the stars of these points have two, three, and four elements, respectively. The corresponding stars are H

$\{(\frac{1}{3}, \frac{1}{3}, \frac{1}{2}), (\frac{2}{3}, \frac{2}{3}, \frac{1}{2})\}$, $L \{(\frac{1}{2}, 0, \frac{1}{2}), (0, \frac{1}{2}, \frac{1}{2}), (\frac{1}{2}, \frac{1}{2}, \frac{1}{2})\}$, and $P \{(\frac{1}{3}, \frac{1}{3}, \frac{1}{3}), (\frac{2}{3}, \frac{2}{3}, \frac{1}{3}), (\frac{1}{3}, \frac{1}{3}, \frac{2}{3}), (\frac{2}{3}, \frac{2}{3}, \frac{2}{3})\}$. The elements of a star correspond to distinct directions that span the subspace of all atomic displacements generated by the eigenvector of the unstable phonon mode. The phonon instabilities at H , L , and P have the irreducible representations (irreps) H_3 , L_2^- , and P_1 , respectively. The isotropy subgroups of an irrep enumerate all possible low-symmetry space groups that can arise out of the corresponding phonon instability, and Table I lists the isotropy subgroups and the associated order parameter directions due to these instabilities. I used the calculated eigenvectors of the unstable phonon modes to generate all these structures. Thus generated structures were then fully relaxed by minimizing both lattice stresses and atomic forces. Relaxation takes a structure to the local minimum in the manifold of the energy landscape defined by the respective order parameter direction.

The calculated total energies of the distorted structures corresponding to the isotropy subgroups obtained after structural relaxations are also given in Table I relative to the energy of the parent $P6/mmm$ phase. In agreement with the finding of Tan and Yan [25], the $H_3(a, 0)$ distortion which also belongs to the space group $P6/mmm$ has the lowest energy. However, I was able to stabilize several more distorted structures, although not all possible isotropy subgroups due to the H_3 , L_2^- , and P_1 instabilities could be stabilized during structural relaxation. The unstable order parameters presumably lie at local maxima or saddle points in the energy landscape, and they relaxed to one of the higher-symmetry phases during the relaxation process.

There are three isotropy subgroups of the H_3 irrep, out of which the $P6/mmm$ $H_3(a, 0)$ and $P6_3/mmc$ $H_3(0, a)$ structures could be stabilized with energies of -16.68 and -10.64 meV/f.u., respectively, relative to that of the parent structure. Six isotropy subgroups belong to the L_2^- irrep, but only three of them maintained their symmetry during the structural relaxation. They are $Immm$ $L_2^-(a, 0, 0)$, $Fm\bar{3}m$ $L_2^-(a, a, a)$, and $P6/mmm$ $L_2^-(a, -a, 0)$ with relative energies of -12.10 , -4.01 , and -7.50 meV/f.u., respectively.

The P_1 irrep has seven isotropy subgroups, but only structures belonging to the $R\bar{3}m$ $P_1(a, 0, 0, 0)$, $P6/mmm$ $P_1(a, 0, a, 0)$, and $P6mm$ $P_1(a, b, a, b)$ subgroups remained stable during relaxation. Interestingly, for each of these three subgroups, two distinct structures could be stabilized that are characterized by order parameters that are out-of-phase by 180° . The out-of-phase pairs occur at different magnitudes of the order parameter, which indicates the presence of local minima at asymmetric positions in the energy landscape defined by the order parameter subspace. This can happen because odd-order terms are allowed by symmetry in the polynomial expansion of the free energy as a function of the order parameters associated with the P_1 irrep, while only even-order terms are allowed for those of H_3 and L_2^- irreps. Nevertheless, the presence of odd-order terms only guarantees

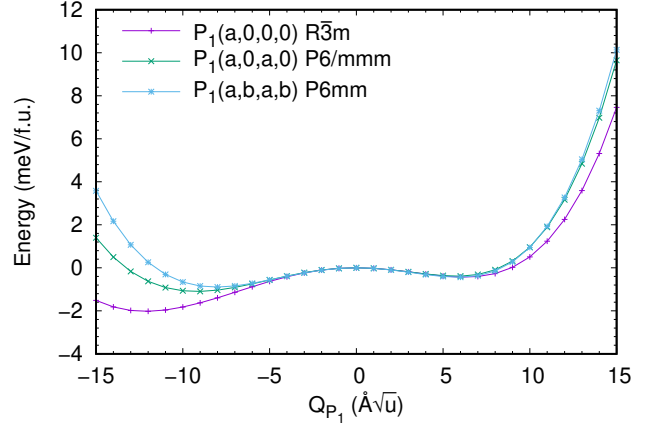


FIG. 2. Calculated energy curves of ScV_6Sn_6 along three different order parameter directions due to the P_1 instability illustrating the presence of six symmetrically-distinct local minima. The energy curves are asymmetric due to the presence of odd-order terms in the free energy. For $P_1(a, b, a, b)$, $b = a \cos(75^\circ)$ has been used that gives the deepest local minimum. Note that the total energies of the structures at the local minima are further lowered and arrive at the values given in Table I after structural relaxations.

that energy surface be asymmetric with respect to the order parameter direction and does not necessitate multiple minima. Therefore, the occurrence three out-of-phase pairs at different values of the order parameters in the energy landscape is noteworthy. Fig. 2 shows the energy curves along the order parameter directions $P_1(a, 0, 0, 0)$, $P_1(a, 0, a, 0)$, and $P_1(a, b, a, b)$ that illustrates the presence of six local minima in this manifold.

As one can note from Table I, the calculated total energies of the six distorted phases due to the P_1 instability lies within 2 meV/f.u. of each other, with values ranging from -3.07 to -1.17 meV/f.u. relative to that of the parent phase. Despite this near-degeneracy, these structures can be distinguished by the different values of mode amplitudes for the primary and secondary order parameter directions, which are given in Table II. For example, the two $R\bar{3}m$ phases with the $P_1(a, 0, 0, 0)$ order parameter direction out-of-phase by 180° have amplitudes of 0.1843 and 0.0981 Å for this mode. There is only one nearest-neighbor Sc-Sn distance in the out-of-plane direction in the parent structure, which multiplies into different values in the distorted structures. The three shortest nearest-neighbor distances in these six structures are also given in Table II, and they can also be used to distinguish these structures.

Although the calculated energies of the distorted phases due to the P_1 instability are higher relative to those due to the H_3 and L_2^- instabilities, more nearly-degenerate distinct structures occur in the manifold of the energy landscape generated by P_1 . As a result, there is more phase space for fluctuations in the order parameter subspace of P_1 than in the subspaces of H_3 and

TABLE II. Mode amplitudes (\AA) of the primary and secondary order parameter directions for the six distorted structures that could be stabilized due to the P_1 phonon instability. Γ_1^+ and K_1 are one- and two-dimensional irreps, respectively. The OPD of K_1 is $(a, 0)$ for all structures. $d_{\text{Sc-Sn}}^1$, $d_{\text{Sc-Sn}}^2$, and $d_{\text{Sc-Sn}}^3$ denote the three shortest nearest-neighbor Sc-Sn distances in \AA in increasing order.

Space group	P_1	Γ_1^+	Δ_1	K_1	$d_{\text{Sc-Sn}}^1$	$d_{\text{Sc-Sn}}^2$	$d_{\text{Sc-Sn}}^3$		
	OPD	amplitude	amplitude	OPD	amplitude	amplitude			
$R\bar{3}m$	$(a, 0, 0, 0)$	0.1843	0.0024	—	—	—	2.9108	2.9323	2.9722
$R\bar{3}m$	$(-a, 0, 0, 0)$	0.0981	0.0040	—	—	—	2.9161	2.9368	2.9501
$P6/mmm$	$(a, 0, a, 0)$	0.1477	0.0028	$(a, 0)$	0.0066	0.0060	2.9109	2.9125	2.9334
$P6/mmm$	$(-a, 0, -a, 0)$	0.1287	0.0039	$(a, 0)$	0.0412	0.0028	2.9048	2.9159	2.9330
$P6mm$	(a, b, a, b)	0.1463	0.0028	(a, b)	0.0094	0.0058	2.9103	2.9120	2.9122
$P6mm$	$(-a, -b, -a, -b)$	0.1299	0.0038	(a, b)	0.0389	0.0026	2.9032	2.9065	2.9151

L_2^- . The gain in entropy associated with this larger multiplicity can energetically favor ordering at P , in a manner analogous to the order-by-disorder mechanism discussed in the context of frustrated magnetic systems [37, 38]. The existence of almost degenerate states that are not trivially related by symmetry is a prerequisite for this phenomenon, and the heuristic argument made here should be confirmed by more rigorous Monte Carlo simulations or field theoretical studies.

Mozaffari *et al.* observe a sublinear relationship $\rho_{xx} \propto T^{0.62}$ between longitudinal resistivity ρ_{xx} and temperature T in ScV_6Sn_6 above the CDW transition, which they ascribe to enhanced scattering of charge carriers in Dirac band by high density of electrons residing at the van Hove singularities that slightly below the Fermi level [39]. However, such van Hove singularities also exist in the electronic structure of the closely related compound LuV_6Sn_6 , but this material does not exhibit sublinear resistivity. Therefore, scattering between electrons in the dispersive Dirac and flat van Hove bands are likely not the cause of sublinear resistivity in ScV_6Sn_6 . Meanwhile, sublinear resistivity is also observed in the vanadium kagome materials AV_3Sb_5 ($A = \text{K, Rb, Cs}$) that exhibit a CDW instability [39–42]. Calculations show that nearly-degenerate distorted phases also occur in these materials [43]. This suggests that scattering of charge carriers with structural fluctuations among the competing phases may lead to sublinear resistivity.

The CDW phase of ScV_6Sn_6 has been variously refined to $R32$ [14] and $R\bar{3}m$ [20] space groups from separate x-ray diffraction studies. The difficulty in resolving the low-temperature structure might be due to freezing in of competing phases. There are two, three, and six possible domains within each xy plane due to the $R\bar{3}m$ $P_1(a, 0, 0, 0)$, $P6/mmm$ $P_1(a, 0, a, 0)$, and $P6mm$ $P_1(a, b, a, b)$ order parameters, respectively, while the $R32$ $P_1(a, 0, 0, 0) + P_2(b, 0, 0, 0)$ order parameter can lead to four different in-plane domains. [Multiplication of each of these numbers by three gives the total number of domains due to different stackings.] Therefore, counting the number of domains that are present in a sample can verify the existence of multiple nearly-degenerate minima proposed here. The $P6mm$ $P_1(a, b, a, b)$ phase lacks

the inversion symmetry, and the observation of a second harmonic generation signal would also support the occurrence of this phase. A more robust test would be the presence of multiple peaks in the pair distribution function due to different nearest-neighbor distances, which would also manifest as different structure factor for the diffraction peaks lying in different Brillouin zones. NMR experiments would be another useful probe because different order parameters due to the P_1 instability lead to different numbers of splitting of the Wyckoff positions.

Hu *et al.* have noted the existence of a nearly flat dispersion of the soft phonon branch in the region around H as it collapses near the CDW transition, and they instead propose that fluctuations in the reciprocal space around H stabilizes the instability at P [44]. They point out that the fluctuations are suppressed at P due to the presence of a cubic term in the polynomial expansion of the free energy, although they do not discuss the occurrence of multiple nontrivially related minima in the energy landscape due to the odd-order nonlinearity. In principle, their theory is complementary to the one proposed in the present study, although the emphasis on the fluctuations about H is hard to reconcile with the disappearance of diffuse signals around H in diffuse scattering experiments.

IV. SUMMARY AND CONCLUSIONS

In summary, I have used first principles calculations to map out the energy landscape of the structural distortions in ScV_6Sn_6 due to the phonon instabilities present in its high-temperature $P6/mmm$ phase. Consistent with previous theoretical and experimental studies, the calculated phonon dispersions show a nondegenerate branch that is unstable along the path L - H and at P , with the instability at H being the dominant one. I used group theoretical analysis to enumerate all possible distortions due to the instabilities at H , L , and P , and generated corresponding structures using the calculated phonon eigenvectors. Structural relaxations show that distortions due to the instabilities at H and L have lower calculated total energies than the ones due to the insta-

bility at P , which is the wave vector where the CDW order condenses. However, I find that energy landscape in the submanifold defined by the order parameter of the P instability is shallower than those due to the H and L instabilities. Only two and three symmetrically-distinct distorted structures are stable at H and L that are spread within the energy ranges of 6 and 5 meV/f.u., respectively. However, I was able to stabilize six different structures due to the instability at P whose relative energies lie within 2 meV/f.u. of each other.

The presence of a larger number of almost degenerate distorted structures at P likely provides the requisite entropic force to cause the first-order CDW transition experimentally observed in ScV_6Sn_6 at this wave vector via the order-by-disorder mechanism, and the heuristic sug-

gestion made here should be confirmed by more rigorous theoretical studies. The energetically shallow manifold of distortions at P could also be verified experimentally, for example, by the presence of more than two inplane domains in the low-temperature phase or the presence of multiple peaks in the pair distribution function due to different nearest-neighbor distances.

V. ACKNOWLEDGEMENTS

I am grateful to Santiago Blanco-Canosa and Benoît Fauqué for insightful discussions. This work was supported by GENCI-TGCC under grant no. A0110913028.

-
- [1] P. Mendels and F. Bert, Quantum kagome frustrated antiferromagnets: One route to quantum spin liquids, *Comptes Rendus Physique* **17**, 455 (2016).
 - [2] W. Beugeling, J. C. Everts, and C. Morais Smith, Topological phase transitions driven by next-nearest-neighbor hopping in two-dimensional lattices, *Phys. Rev. B* **86**, 195129 (2012).
 - [3] W. R. Meier, M.-H. Du, S. Okamoto, N. Mohanta, A. F. May, M. A. McGuire, C. A. Bridges, G. D. Samolyuk, and B. C. Sales, Flat bands in the cosn-type compounds, *Phys. Rev. B* **102**, 075148 (2020).
 - [4] M. Kang, L. Ye, S. Fang, J.-S. You, A. Levitan, M. Han, J. I. Facio, C. Jozwiak, A. Bostwick, E. Rotenberg, M. K. Chan, R. D. McDonald, D. Graf, K. Kaznatcheev, E. Vescovo, D. C. Bell, E. Kaxiras, J. van den Brink, M. Richter, M. P. Ghimire, J. G. Checkelsky, and R. Comin, Dirac fermions and flat bands in the ideal kagome metal FeSn , *Nature Materials* **19**, 163 (2019).
 - [5] Z. Liu, M. Li, Q. Wang, G. Wang, C. Wen, K. Jiang, X. Lu, S. Yan, Y. Huang, D. Shen, J.-X. Yin, Z. Wang, Z. Yin, H. Lei, and S. Wang, Orbital-selective dirac fermions and extremely flat bands in frustrated kagome-lattice metal CoSn , *Nature Communications* **11**, 4002 (2020).
 - [6] H.-M. Guo and M. Franz, Topological insulator on the kagome lattice, *Phys. Rev. B* **80**, 113102 (2009).
 - [7] A. Rüegg and G. A. Fiete, Fractionally charged topological point defects on the kagome lattice, *Phys. Rev. B* **83**, 165118 (2011).
 - [8] E. Tang, J.-W. Mei, and X.-G. Wen, High-temperature fractional quantum hall states, *Phys. Rev. Lett.* **106**, 236802 (2011).
 - [9] W.-S. Wang, Z.-Z. Li, Y.-Y. Xiang, and Q.-H. Wang, Competing electronic orders on kagome lattices at van hove filling, *Phys. Rev. B* **87**, 115135 (2013).
 - [10] M. L. Kiesel, C. Platt, and R. Thomale, Unconventional fermi surface instabilities in the kagome hubbard model, *Phys. Rev. Lett.* **110**, 126405 (2013).
 - [11] I. Mazin, H. O. Jeschke, F. Lechermann, H. Lee, M. Fink, R. Thomale, and R. Valentí, Theoretical prediction of a strongly correlated dirac metal, *Nature communications* **5**, 4261 (2014).
 - [12] B. R. Ortiz, L. C. Gomes, J. R. Morey, M. Winiarski, M. Bordelon, J. S. Mangum, I. W. H. Oswald, J. A. Rodriguez-Rivera, J. R. Neilson, S. D. Wilson, E. Ertekin, T. M. McQueen, and E. S. Toberer, New kagome prototype materials: discovery of kv_3sb_5 , rbv_3sb_5 , and csv_3sb_5 , *Phys. Rev. Mater.* **3**, 094407 (2019).
 - [13] X. Teng, L. Chen, F. Ye, E. Rosenberg, Z. Liu, J.-X. Yin, Y.-X. Jiang, J. S. Oh, M. Z. Hasan, K. J. Neubauer, *et al.*, Discovery of charge density wave in a kagome lattice antiferromagnet, *Nature* **609**, 490 (2022).
 - [14] H. W. Suriya Arachchige, W. R. Meier, M. Marshall, T. Matsuoka, R. Xue, M. A. McGuire, R. P. Hermann, H. Cao, and D. Mandrus, Charge density wave in kagome lattice intermetallic scv_6sn_6 , *Phys. Rev. Lett.* **129**, 216402 (2022).
 - [15] M. Tuniz, A. Consiglio, D. Puntel, C. Bigi, S. Enzner, G. Pokharel, P. Orgiani, W. Bronsch, F. Parmigiani, V. Polewczyk, P. D. C. King, J. W. Wells, I. Zeljkovic, P. Carrara, G. Rossi, J. Fujii, I. Vobornik, S. D. Wilson, R. Thomale, T. Wehling, G. Sangiovanni, G. Panaccione, F. Cilento, D. Di Sante, and F. Mazzola, Dynamics and resilience of the charge density wave in a bilayer kagome metal, *arXiv:2302.10699 [cond-mat.str-el]* (2023).
 - [16] S. Cheng, Z. Ren, H. Li, J. Oh, H. Tan, G. Pokharel, J. M. DeStefano, E. Rosenberg, Y. Guo, Y. Zhang, Z. Yue, Y. Lee, S. Gorovikov, M. Zonno, M. Hashimoto, D. Lu, L. Ke, F. Mazzola, J. Kono, R. J. Birgeneau, J.-H. Chu, S. D. Wilson, Z. Wang, B. Yan, M. Yi, and I. Zeljkovic, Nanoscale visualization and spectral fingerprints of the charge order in scv_6sn_6 distinct from other kagome metals, *arXiv:2302.12227 [cond-mat.str-el]* (2023).
 - [17] S.-H. Kang, H. Li, W. R. Meier, J. W. Villanova, S. Hus, H. Jeon, H. W. S. Arachchige, Q. Lu, Z. Gai, J. Denlinger, R. Moore, M. Yoon, and D. Mandrus, Emergence of a new band and the lifshitz transition in kagome metal scv_6sn_6 with charge density wave, *arXiv:2302.14041 [cond-mat.str-el]* (2023).
 - [18] T. Hu, H. Pi, S. Xu, L. Yue, Q. Wu, Q. Liu, S. Zhang, R. Li, X. Zhou, J. Yuan, D. Wu, T. Dong, H. Weng, and N. Wang, Optical spectroscopy and band structure calculations of the structural phase transition in the vanadium-based kagome metal scv_6sn_6 , *Phys. Rev.*

- B 107**, 165119 (2023).
- [19] Y. Hu, J. Ma, Y. Li, D. J. Gawryluk, T. Hu, J. Teyssier, V. Multian, Z. Yin, Y. Jiang, S. Xu, S. Shin, I. Plokhikh, X. Han, N. C. Plumb, Y. Liu, J. Yin, Z. Guguchia, Y. Zhao, A. P. Schnyder, X. Wu, E. Pomjakushina, M. Z. Hasan, N. Wang, and M. Shi, Phonon promoted charge density wave in topological kagome metal ScV_6Sn_6 , [arXiv:2304.06431 \[cond-mat.str-el\]](#) (2023).
- [20] A. Korshunov, H. Hu, D. Subires, Y. Jiang, D. Călugăru, X. Feng, A. Rajapitamahuni, C. Yi, S. Roychowdhury, M. G. Vergniory, J. Strempfer, C. Shekhar, E. Vescovo, D. Chernyshov, A. H. Said, A. Bosak, C. Felser, B. A. Bernevig, and S. Blanco-Canosa, Softening of a flat phonon mode in the kagome ScV_6Sn_6 , [arXiv:2304.09173 \[cond-mat.str-el\]](#) (2023).
- [21] S. Lee, C. Won, J. Kim, J. Yoo, S. Park, J. Denlinger, C. Jozwiak, A. Bostwick, E. Rotenberg, R. Comin, M. Kang, and J.-H. Park, Nature of charge density wave in kagome metal ScV_6Sn_6 , [arXiv:2304.11820 \[cond-mat.str-el\]](#) (2023).
- [22] D. Di Sante, C. Bigi, P. Eck, S. Enzner, A. Consiglio, G. Pokharel, P. Carrara, P. Orgiani, V. Polewczyk, J. Fujii, P. D. C. King, I. Vobornik, G. Rossi, I. Zeljkovic, S. D. Wilson, R. Thomale, G. Sangiovanni, G. Panaccione, and F. Mazzola, Flat band separation and robust spin berry curvature in bilayer kagome metals, *Nature Physics* **10.1038/s41567-023-02053-z** (2023).
- [23] S. Cao, C. Xu, H. Fukui, T. Manjo, M. Shi, Y. Liu, C. Cao, and Y. Song, Competing charge-density wave instabilities in the kagome metal ScV_6Sn_6 , [arXiv:2304.08197 \[cond-mat.str-el\]](#) (2023).
- [24] G. Pokharel, B. R. Ortiz, L. Kautzsch, S. J. G. Alvarado, K. Mallayya, G. Wu, E.-A. Kim, J. P. C. Ruff, S. Sarker, and S. D. Wilson, Frustrated charge order and cooperative distortions in scv6sn6 (2023), [arXiv:2307.11843 \[cond-mat.str-el\]](#).
- [25] H. Tan and B. Yan, Abundant lattice instability in kagome metal ScV_6Sn_6 , [arXiv:2302.07922 \[cond-mat.mtrl-sci\]](#) (2023).
- [26] P. Giannozzi, O. Andreussi, T. Brumme, O. Bunau, M. B. Nardelli, M. Calandra, R. Car, C. Cavazzoni, D. Ceresoli, M. Cococcioni, N. Colonna, I. Carnimeo, A. D. Corso, S. de Gironcoli, P. Delugas, R. A. DiStasio, A. Ferretti, A. Floris, G. Fratesi, G. Fugallo, R. Gebauer, U. Gerstmann, F. Giustino, T. Gorni, J. Jia, M. Kawamura, H.-Y. Ko, A. Kokalj, E. Küçükbenli, M. Lazzeri, M. Marsili, N. Marzari, F. Mauri, N. L. Nguyen, H.-V. Nguyen, A. O. de-la Roza, L. Paulatto, S. Poncé, D. Rocca, R. Sabatini, B. Santra, M. Schlipf, A. P. Seitsonen, A. Smogunov, I. Timrov, T. Thonhauser, P. Umari, N. Vast, X. Wu, and S. Baroni, Advanced capabilities for materials modelling with quantum espresso, *Journal of Physics: Condensed Matter* **29**, 465901 (2017).
- [27] A. M. J. Klimeš, D. R. Bowler, Chemical accuracy for the van der waals density functional, *Journal of Physics: Condensed Matter* **22**, 022201 (2009).
- [28] A. Dal Corso, Pseudopotentials periodic table: From H to Pu, *Computational Materials Science* **95**, 337 (2014).
- [29] S. Baroni, S. de Gironcoli, A. Dal Corso, and P. Giannozzi, Phonons and related crystal properties from density-functional perturbation theory, *Rev. Mod. Phys.* **73**, 515 (2001).
- [30] H. T. Stokes, B. J. Campbell, and D. M. Hatch, ISOTROPY software suite, [iso.byu.edu](#).
- [31] H. T. Stokes and D. M. Hatch, FINDSYM: program for identifying the space-group symmetry of a crystal, *Journal of Applied Crystallography* **38**, 237 (2005).
- [32] A. Togo and I. Tanaka, SPGLIB: a software library for crystal symmetry search, [arXiv:1808.01590 \[cond-mat.mtrl-sci\]](#) (2018).
- [33] D. Orobengoa, C. Capillas, M. I. Aroyo, and J. M. Perez-Mato, AMPLIMODES: symmetry-mode analysis on the Bilbao crystallographic server, *Journal of Applied Crystallography* **42**, 820 (2009).
- [34] D. M. Hatch and H. T. Stokes, INVARIANTS: program for obtaining a list of invariant polynomials of the order-parameter components associated with irreducible representations of a space group, *Journal of Applied Crystallography* **36**, 951 (2003).
- [35] See Supplemental Material for full structural information of all the phases discussed in the paper.
- [36] Y. Gu, E. Ritz, W. R. Meier, A. Blockmon, K. Smith, R. P. Madhugaria, S. Mozaffari, D. Mandrus, T. Birol, and J. L. Musfeldt, Origin and stability of the charge density wave in ScV_6Sn_6 , [arXiv:2305.01086 \[cond-mat.str-el\]](#) (2023).
- [37] J. Villain, R. Bidaux, J.-P. Carton, and R. Conte, Order as an effect of disorder, *J. Phys. France* **41**, 1263 (1980).
- [38] A. Chubukov, Order from disorder in a kagome antiferromagnet, *Journal of Applied Physics* **73**, 5639 (1993).
- [39] S. Mozaffari, W. R. Meier, R. P. Madhugaria, S.-H. Kang, J. W. Villanova, H. W. S. Arachchige, G. Zheng, Y. Zhu, K.-W. Chen, K. Jenkins, D. Zhang, A. Chan, L. Li, M. Yoon, Y. Zhang, and D. G. Mandrus, Universal sublinear resistivity in vanadium kagome materials hosting charge density waves (2023), [arXiv:2305.02393 \[cond-mat.str-el\]](#).
- [40] B. R. Ortiz, P. M. Sarte, E. M. Kenney, M. J. Graf, S. M. L. Teicher, R. Seshadri, and S. D. Wilson, Superconductivity in the \mathbb{Z}_2 kagome metal KV_3Sb_5 , *Phys. Rev. Mater.* **5**, 034801 (2021).
- [41] Q. Yin, Z. Tu, C. Gong, Y. Fu, S. Yan, and H. Lei, Superconductivity and normal-state properties of kagome metal rbv3sb5 single crystals, *Chinese Physics Letters* **38**, 037403 (2021).
- [42] B. R. Ortiz, S. M. L. Teicher, Y. Hu, J. L. Zuo, P. M. Sarte, E. C. Schueller, A. M. M. Abeykoon, M. J. Krogstad, S. Rosenkranz, R. Osborn, R. Seshadri, L. Balents, J. He, and S. D. Wilson, Cv_3sb_5 : A F_2 topological kagome metal with a superconducting ground state, *Phys. Rev. Lett.* **125**, 247002 (2020).
- [43] A. Subedi, Hexagonal-to-base-centered-orthorhombic $4Q$ charge density wave order in kagome metals KV_3Sb_5 , RbV_3Sb_5 , and CsV_3Sb_5 , *Phys. Rev. Mater.* **6**, 015001 (2022).
- [44] H. Hu, Y. Jiang, D. Călugăru, X. Feng, D. Subires, M. G. Vergniory, C. Felser, S. Blanco-Canosa, and B. A. Bernevig, Kagome materials I: $\text{Sg } 191$, ScV_6Sn_6 . Flat Phonon Soft Modes and Unconventional CDW Formation: Microscopic and Effective Theory, [arXiv:2305.15469 \[cond-mat.str-el\]](#) (2023).